[12] M. Bosiljevac, M. Casaletti, F. Caminita, Z. Sipus, and S. Maci, "Highly tapered, uniform phased horn based on variable impedance lens effect," in *Proc. EuCAP*, Rome, Italy, Apr. 11–15, 2011, pp. 3683–3686.
[13] B. Zhou and T. J. Cui, "Directivity enhancement to Vivaldi antennas using compactly anisotropic zero-index metamaterials," *IEEE Antennas Wireless Propag. Lett.*, vol. 10, pp. 326–329, 2011.
[14] M. Sun, Z. N. Chen, and X. Qing, "Gain enhancement of 60-GHz antipodal tapered slot antenna using zero-index metamaterial," *IEEE Trans. Antennas. Propag.*, vol. 61, no. 1, pp. 1741–1746, 2013.
[15] W. Cao, B. Zhang, A. Liu, T. Yu, D. Guo, and Y. Wei, "Gain enhancement for broadband periodic endfire antenna by using split-ring resonator structures," *IEEE Trans. Antennas. Propag.*, vol. 60, no. 7, pp. 3513–3516, 2012.
[16] W. Cao, B. Zhang, A. Liu, T. Yu, D. Guo, and Y. Wei, "Broadband high-gain periodic endfire antenna by using I-shaped resonator (ISR) structures," *IEEE Antennas Wireless Propag. Lett.*, vol. 11, pp. 1470–1473, 2012.
[17] R. Liu, Q. Cheng, J. Y. Chin, J. J. Mock, T. J. Cui, and D. R. Smith, "Broadband gradient index microwave quasi-optical elements based on non-resonant metamaterials," *Opt. Express*, vol. 17, no. 23, pp. 21030–21041, 2009.
[18] Z. L. Mei, J. Bai, T. M. Niu, and T. J. Cui, "A half Maxwell fish-eye lens antenna based on gradient-index metamaterials," *IEEE Trans. Antennas. Propag.*, vol. 60, no. 1, pp. 398–401, 2012.
[19] R. Yang, Z. Lei, L. Chen, J. Zhang, Z. Wang, and Y. Xie, "Broadband converging plano-concave lens," *Opt. Lett.*, vol. 38, no. 13, pp. 2311–2313, 2013.
[20] D. R. Smith, D. C. Vier, T. Koschny, and C. M. Soukoulis, "Electromagnetic parameter retrieval from inhomogeneous metamaterials," *Phys. Rev. E*, vol. 71, no. 3, p. 036617, 2005.

Statistical On-Body Measurement Results at 60 GHz

Luca Petrillo, Theodoros Mavridis, Julien Sarrazin, Aziz Benlarbi-Delaï, and Philippe De Doncker

***Abstract*—This communication studies the path loss and shadowing between two body mounted devices at 60 GHz. The temporal fading is experimentally investigated and the Doppler spectrum is characterized and modeled. Measurements have been conducted in an anechoic chamber for both horizontal and vertical polarizations.**

***Index Terms*—60 GHz propagation, body area networks (BAN), channel model.**

I. Introduction

Future wireless body area networks (WBAN) will allow a variety of applications ranging from health care to entertainment or defense. Researches in the past years have been mainly concentrated on communicating systems working around 2.4 GHz [1] and in the ultra wideband (UWB) spectrum [2] because of the wide availability of the devices. Nowadays, the emergence of 60 GHz communicating systems [3] encourages the study and development of new 60 GHz body area networks (BAN) [4]. Specific on-body 60 GHz channels have been investigated [5], [6] and some preliminary results for path gain on the body have been presented [7]. Static propagation models for off-body [8] and on-body [9] 60 GHz communications have already been studied and a skin-equivalent phantom at 60 GHz has been proposed to validate plane-propagation models [10]. This communication proposes an experimental study to characterize path loss and shadowing between two body mounted devices and the fading due to breathing at 60 GHz. Due to the high attenuation at this frequency, high fading phenomena are expected.

Manuscript received December 03, 2013; revised September 04, 2014; accepted October 12, 2014. Date of publication October 23, 2014; date of current version December 31, 2014. This work was performed within the Labex SMART supported by French state funds managed by the ANR within the Investissements d'Avenir programme under reference ANR-11-IDEX-0004-02.

L. Petrillo, T. Mavridis, and P. De Doncker are with OPERA Dpt.—Wireless Communications Group, Université Libre de Bruxelles (ULB), B-1050 Brussels, Belgium (e-mail: lpetrill@ulb.ac.be; tmavridi@ulb.ac.be; pdedonck@ulb.ac.be).

T. Mavridis, J. Sarrazin, and A. Benlarbi-Delaï are with L2E Dept., Sorbonne Universités, UPMC Univ Paris 06, UR2, L2E, F-75005, Paris, France (e-mail: julien.sarrazin@upmc.fr; aziz.benlarbi_delai@umpc.fr).

Color versions of one or more of the figures in this communication are available online at http://ieeexplore.ieee.org.

Digital Object Identifier 10.1109/TAP.2014.2364611

II. Measurement Campaign

The experimental campaign has been conducted on a person, with the characteristics presented in Table I, in an anechoic chamber to avoid any environment influence. The person under test (PUT) is a male wearing a cotton t-shirt. An Agilent E8361C Vector Network Analyser (VNA) and U-Band open wave-guide antennas have been used. We ensured that the open waveguides were oriented towards each other while collecting measurements, in order to prevent mis-alignment. Effects of small mis-alignments, which cannot be avoided, is palliated by the relative large beamwidth of open waveguides used as antennas in the azimuthal direction. To reduce the losses in the cables and reduce their lengths, the VNA has been placed inside the anechoic chamber and delivers a transmitted power of 0 d Bm. A power amplifier with a gain of 30 dB at 60 GHz has been used at transmission side to raise link budget. The VNA has been used on continuous wave mode.

Measurements have been performed for both vertical (normal to the body surface) and horizontal (longitudinal to the body surface) polarizations, and for five particular distances between antennas: 5, 10, 15, 20 and 25 cm. For each distance, we took different realizations of the measurements: vertical and horizontal links, with respect to the human body, were investigated, so that for each distance and for each polarization we took forty measurements. The positions have been chosen in order to have equal numbers of measurement on the chest and on the abdomen, as well as vertical and horizontal links. So, for example, for vertical polarization and for 5 cm between the antennas, we measured 10 vertical and 10 horizontal links on the chest, 10 vertical and 10 horizontal links on the abdomen. For 20 and 25 cm distances, vertical measurements correspond to 20 chest-abdomen links. For the distance 25 cm, horizontal measurements have not been taken, since the torso of the PUT was not sufficiently large to obtain such distance. A scheme is shown in Fig. 1, where stars linked by a dashed line indicate a measure for a particular distance, place on the PUT and orientation of the link. We have schematically indicated chest and abdomen by an horizontal line representing the diaphragm.

Each measurement has been conducted during 10 seconds which is equivalent to 150 temporal acquisitions. The antennas were located at 2 cm from the body surface for both transmitter (TX) and receiver (RX) antenna. This choice permits to compare the influence of antenna body separation by comparison with [11]. The measurement parameters are summarized in Table II.

TABLE I
PHYSICAL QUANTITIES OF THE BODY

Quantity	Value
Gender	Male
Height	172 cm
Weight	60 Kg
Torso Perimeter	86 cm

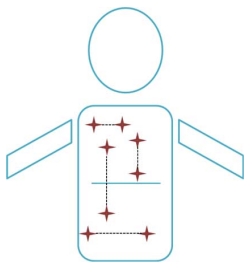

Fig. 1. Measurement scheme. Stars correspond to measurement points on the front of torso. We depicted horizontal and vertical links of different lengths, on the chest, on the abdomen and one vertical chest-abdomen link. The horizontal line represents diaphragm and separate chest from abdomen.

TABLE II
PARAMETERS OF THE MEASUREMENT CAMPAIGN

Symbol	Value
f	60 GHz
Measurement time	10 s
Acquisitions per measurement	150
Body-antenna distance	2 cm
Reference distances	5, 10, 15, 20 and 25 cm

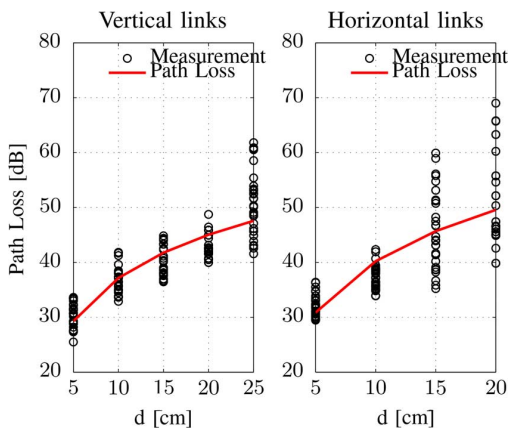

Fig. 2. Measurement results for vertical polarization, vertical and horizontal links. The dots stand for time averaged measurement and the solid line for the path loss.

III. ON-BODY PATH LOSS

A. Measurement Results and Path Loss Model

In the following, the experimental results are averaged over time and each measurement is presented as the mean value over the 150 time acquisitions.

Vertical Polarization: The path loss for vertical and horizontal links for vertical polarization are shown in Fig. 2.

The path loss L_{dB} can be easily modeled with distance d as a logarithmic path loss:

$$L_{\mathrm{dB}}(d) = L^0_{\mathrm{dB}} + 10n\log_{10}(d/d_0) \quad (1)$$

TABLE III
PATH LOSS PARAMETERS FOR VERTICAL AND HORIZONTAL LINKS FOR VERTICAL POLARIZATION

Vertical links	Horizontal links
d_0=5 cm	d_0=5 cm
L^0=29.3 dB	L^0=30.87 dB
n=2.62	n=3.1
$d \leq$20 cm	$d \leq$10 cm
σ_L=2.36 dB	σ_L=2.13 dB
$d =$25 cm	$d \geq$15 cm
σ_L=5.85 dB	σ_L=7.68 dB

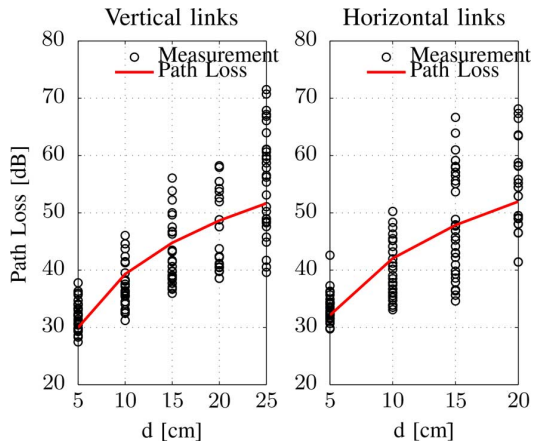

Fig. 3. Measurement results for horizontal polarization, vertical and horizontal links. The dots stand for time averaged measurement and the solid line for the path loss.

where d_0 is a reference distance, L^0_{dB} is the path loss at d_0 and n is the path loss exponent. Shadowing can be modeled by a random variable following normal distribution, with zero mean and standard deviation σ_L. We propose for both vertical and horizontal links two values of σ_L, depending on the distance range. Model parameters are summarized in Table III.

It can be deduced that the electromagnetic waves attenuate faster for horizontal links. The reason is that for horizontal links, the surface of propagation is more curved than for vertical ones because of the human body shape, and therefore diffraction is more severe. Moreover, measurements are more scattered for horizontal links, which is also a consequence of diffraction. For vertical links, it can be considered that the main propagation mechanism is the sum of direct and reflected waves off the flat surface of the body between the antennas. Constructive and destructive interference between these two contributions can be significant. With respect to measurement results presented in this section, path-loss as function of distance seems not to be useful due to high dispersion of measurement points. For both vertical and horizontal links, high standard deviation values arise because line-of-sight between the open waveguides can be obstructed by torso curvature (for horizontal links) or by stomach sphericity (for vertical links).

Horizontal Polarization: The path loss for vertical and horizontal links for horizontal polarization is shown in Fig. 3.

Again, the path loss model is given by (1) and path loss coefficients are given in Table IV. As compared to vertical polarization, horizontal polarization measurements show greater standard deviation, as is commonly found in lower frequency BAN channel measurements [12]. This can be explained by the reflected wave

TABLE IV
PATH LOSS PARAMETERS FOR VERTICAL AND HORIZONTAL LINKS FOR HORIZONTAL POLARIZATION

Vertical links	Horizontal links
d_0=5 cm L^0=29.98 dB n=3.10	d_0=5 cm L^0=32.14 dB n=3.29
$d \geq$5 cm σ_L=2.61+0.3(d-5) dB	$d \leq$10 cm σ_L=3.77 dB
	$d \geq$15 cm σ_L=8.27 dB

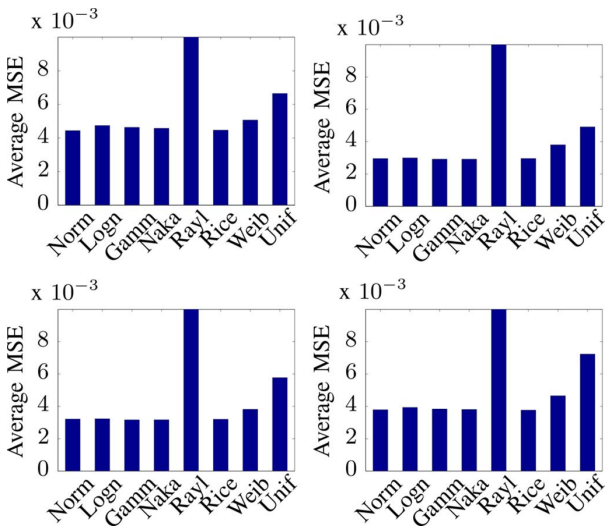

Fig. 4. Average MSE of common distribution fits. The above row presents the vertical polarization and the below row presents the horizontal polarization. The left column is the vertical links while the right column is the horizontal links.

influence on the total received field, which, for horizontal polarization, is more pronounced than for vertical polarization [11]. Norton's formulations [13] predict this trend for Hertzian dipoles placed several wavelengths above a conductive surface. It is shown that the combination between direct and reflected waves on the body surface gives a more oscillating pattern for horizontal polarization with respect to spatial parameters. For vertical links, the standard deviation linearly increase at the rate of 0.3 dB/cm, from a first value equal to 2.61 dB found at 5 cm. For horizontal links the trend is even worse due to the adverse effects of body curvature. Regardless of polarization, measurement results suggest that path-loss for on-body channel links on the front side of the torso at 60 GHz is not useful to describe radio channel because of too high variability of measurement points around the fitting. This is due to the small wavelength at 60 GHz that significantly affects the channel spatial variation due to different spots of transmitter and receiver on the torso. We are of the opinion that point-to-point scenario analysis should be used instead.

IV. TEMPORAL FADING

To study temporal fading, different distributions (Normal, Lognormal, Gamma, Nakagami, Rayleigth, Rice, Weibull and Uniform) were investigated. For each model, estimation results were evaluated through mean square error (MSE). Results are plotted in Fig. 4. Lognormal distribution is then adopted, which permits to represent temporal fading in dB by a normal distribution. The standard deviation

TABLE V
NORMAL FADING PARAMETERS

Channel	n_{σ_F}	σ_{F_0}	σ_{sigma_F}
V. Pol. V. links	0.028	0.53	0.67
V. Pol. H. links	0.073	0.43	0.98
H. Pol. V links	0.053	0.66	1.15
H. Pol. H links	0.086	0.35	0.9

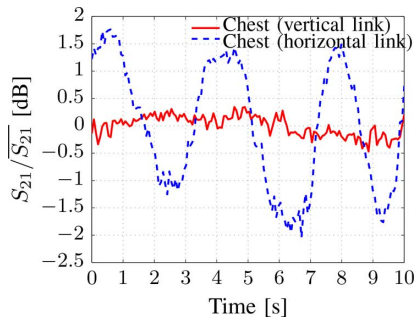

Fig. 5. Channel fading amplitude for two measurement samples of S_{21} normalized by their mean values.

(STD) is evaluated for each polarization, link and distance. It is increasing with the distance, as it has been observed at lower frequency [14]. Therefore, we characterize it by:

$$\sigma_F = \mu_{\sigma_F} + \sigma_{\sigma_F}\mathcal{N}(0,1) \quad (2)$$

$$\mu_{\sigma_F} = \sigma_{F_0} + n_{\sigma_F}(d - d_0). \quad (3)$$

Where $\mathcal{N}(0,1)$ is a normal process of zero mean and variance equal to 1. Values of $n_{\sigma_F}, \sigma_{F_0}, \sigma_{\sigma_F}$ for $d_0 = 5$ cm are reported in Table V.

Due to the small wavelength, on-body channel at 60 GHz on the front side of the torso is subject to dynamical body scattering because of breathing, which cause the thorax and the abdomen to inflate and deflate. Fig. 5 shows two examples of measurements in the temporal domain, normalized with respect to their mean values $\overline{S_{21}}$. The first one (solid line) corresponds to a distance between antennas equal to 15 cm, vertical polarization and vertical link on the chest. This is almost a static channel, where temporal fading follows a normal distribution in logarithmic scale. On the other hand, the dashed line clearly reveals a periodic movement that affects the channel between the antennas : it corresponds to the same 15 cm distance between antennas for the same polarization and for an horizontal link on the chest. The breathing affects the channel, since the chest naturally expands and compress, varying the distance between antennas. A similar effect is experimentally found for vertical links greater than 20 cm (chest-abdomen), caused by stomach's compressing and deflating. For links affected by respiration, the temporal fading is not normally distributed, as it has already been reported in [9] for abdomen/chest links, but its probability density function is almost uniformly distributed.

We are of the opinion that the reason has to be found in the breathing action that affects the channel and consequently Doppler Spectrum needs to be investigated to characterize this phenomenon.

A. Breathing Doppler Characterization

To characterize the Doppler spectrum we took a new set of measurements by increasing the acquisition length, which has been set to 30 sec. Measurements have been taken for both vertical and horizontal polarizations with the same setup as previous measures. We have investigated an horizontal link on the chest and a vertical chest-stomach link. The Doppler spectrum is estimated with the Welch periodogram

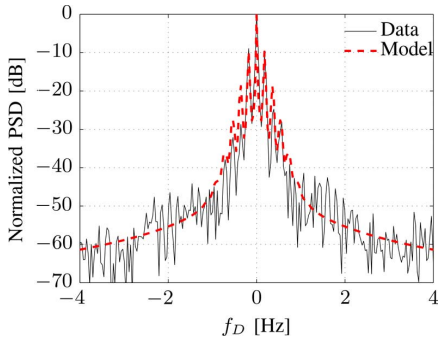

Fig. 6. Normalized Doppler PSD and model of body link affected by breathing influence (vertical polarization, chest).

TABLE VI
DOPPLER PSD ESTIMATION

Measurement	f_0 [Hz]	s $[Hz^{-2}]$	$x[W]$	a
V. Pol. chest	0.18	85980	339	287
H. Pol. chest	0.2	77150	281.9	75.8
V. Pol. chest-abdomen	0.18	81450	933.5	673.7
H. Pol. chest-abdomen	0.25	63840	168.2	11.9

method [15] by normalizing the channel gains to 0 dB. The average Doppler power spectral density (PSD) of a typical body link affected by breathing is shown in Fig. 6: the zero Doppler frequency is found because S_{21} oscillates around a mean value, whereas the peaks are at fundamental frequency, which is nearly 0.18 Hz, and its harmonics. The breathing cycle then lasts approximately 5 sec, which it is considered as normal at rest [16]. Following [17], we propose a model for respiration Doppler PSD:

$$\mathrm{PSD}(f_D) = \frac{1}{1+sf_D^2}\sum_{m=1}^{\infty}\frac{x}{2^m}\frac{1}{1+4^m a+s^2(f_D\pm mf_0)^4} \qquad (4)$$

where f_0 is the breathing frequency and s, x and a are independent parameters of the model whose values are estimated by minimal square error (MSE) estimator. The parameters estimation is shown in Table VI for different torso links.

V. CONCLUSION

In this communication, we presented the results of a measurement campaign conducted at 60 GHz on the front of the torso of a human subject for both vertical and horizontal polarizations. A path loss has been derived for horizontal and vertical links, while large deviations around the models have been observed regardless of polarization. Temporal fading is then discussed and investigated: a normal fit in dB scale is adopted and a model for STD is derived. Doppler spectrum is evaluated and an analytical model is introduced. Estimated parameters are reported.

ACKNOWLEDGMENT

The authors would like to thank Prof. B. Huyart and A. Khy from Telecom ParisTech for their helpful advice and willingness.

REFERENCES

[1] N. F. Timmons and W. G. Scanlon, "Analysis of the performance of IEEE 802.15. 4 for medical sensor body area networking," in *Proc. 1st Annu. IEEE Comm. Society Conf. on Sensor and Ad Hoc Comm. and Networks*, 2004, pp. 16–24, IEEE.

[2] A. Fort, C. Desset, P. De Doncker, P. Wambacq, and L. Van Biesen, "An ultra-wideband body area propagation channel model-from statistics to implementation," *IEEE Trans. Microw. Theory Tech.*, vol. 54, no. 4, pp. 1820–1826, 2006.

[3] T. S. Rappaport, J. N. Murdock, and F. Gutierrez, "State of the art in 60-GHz integrated circuits and systems for wireless communications," *Proc. IEEE*, vol. 99, no. 8, pp. 1390–1436, 2011.

[4] S. Alipour, F. Parvaresh, H. Ghajari, and F. Donald, "Propagation characteristics for a 60 GHz wireless body area network (WBAN)," in *Proc. Military Comm. Conf.*, 2010, pp. 719–723, IEEE.

[5] Y. Nechayev, X. Wu, C. Constantinou, and P. Hall, "Effect of body motion on propagation path gain at 60 GHz," in *Proc. 6th Eur. Conf. on Antennas and Propagation*, 2012, pp. 3397–3401, IEEE.

[6] Y. Nechayev, C. Constantinou, S. Swaisaenyakorn, O. Rakibet, J. Batchelor, P. Hall, C. Parini, and J. Hunt, "Use of motion capture for path gain modelling of millimetre-wave on-body communication links," in *Proc. ISAP2012*, 2012, vol. 3, p. 5.

[7] X. Wu, Y. Nechayev, and P. Hall, "Antenna design and channel measurements for on-body communications at 60 GHz," in *Proc. XXXth URSI General Assembly and Scientific Symp.*, 2011, pp. 1–4, IEEE.

[8] T. Mavridis, L. Petrillo, J. Sarrazin, D. Lautru, A. Benlarbi-Delaï, and P. De Doncker, "Theoretical and experimental investigation of a 60 GHz off-body propagation model," *IEEE Trans. Antennas Propag.*, vol. 62, no. 1, pp. 393–402, 2014.

[9] L. Petrillo, T. Mavridis, J. Sarrazin, D. Lautru, A. Benlarbi-Delaï, and P. De Doncker, "Analytical creeping wave model and measurements for 60 GHz body area networks," *IEEE Trans. Antennas Propag.*, vol. 62, no. 8, pp. 4352–4356, Aug. 2014.

[10] N. Chahat, M. Zhadobov, and R. Sauleau, "Skin-equivalent phantom for on-body antenna measurements at 60 GHz," in *Proc. 6th Eur. Conf. on Antennas Propag. (EUCAP)*, Mar. 2012, pp. 1362–1664.

[11] N. Chahat, G. Valerio, M. Zhadobov, and R. Sauleau, "On-body propagation at 60 GHz," *IEEE Trans. Antennas Propag.*, vol. 61, no. 4, pp. 1876–1888, Apr. 2013.

[12] H. Ghannoum, R. D'Errico, C. Roblin, and X. Begaud, "Characterization of the UWB on-body propagation channel," in *Proc. 1st Eur. Conf. on Antennas and Propagation*, Nov. 2006, pp. 1–6.

[13] R. W. King, G. J. Fikioris, and R. B. Mack, *Cylindrical Antennas and Arrays*. Cambridge, U.K.: Cambridge Univ. Press, 2002.

[14] L. Liu, R. D'Errico, L. Ouvry, P. De Doncker, and C. Oestges, "Dynamic channel modeling at 2.4 GHz for on-body area networks," *Adv. Electron. Telecom.-Radio Comm.*, ser. Recent Advances in Wireless Comm. Networks, vol. 2, no. 4, 2011.

[15] P. D. Welch, "The use of fast Fourier transform for the estimation of power spectra: A method based on time averaging over short, modified periodograms," *IEEE Trans. Audio Electroacoust.*, vol. 15, no. 2, pp. 70–73, 1967.

[16] W. Lindh, M. Pooler, C. Tamparo, B. Dahl, and J. Morris, *Delmar's Comprehensive Medical Assisting: Administrative and Clinical Competencies*. Boston, MA, USA: Cengage Learning, 2013.

[17] L. Liu, S. Van Roy, F. Quitin, P. De Doncker, and C. Oestges, "Statistical characterization and modeling of Doppler spectrum in dynamic on-body channels," *IEEE Antennas Wireless Propag. Lett.*, vol. 12, pp. 186–189, 2013.